

# Resilient Path Planning of UAVs against Covert Attacks on UWB Sensors

Jiayi He<sup>\*1</sup>, Graduate Student Member, IEEE, Xin Gong<sup>\*1</sup>, Graduate Student Member, IEEE, Yukang Cui<sup>2</sup>, Member, IEEE, and Tingwen Huang<sup>3</sup>, Fellow, IEEE

**Abstract**—In this letter, a resilient path planning scheme is proposed to navigate a UAV to the planned (nominal) destination with minimum energy-consumption in the presence of a smart attacker. The UAV is equipped with two sensors, a GPS sensor, which is vulnerable to the spoofing attacker, and a well-functioning Ultra-Wideband (UWB) sensor, which is possible to be fooled. We show that a covert attacker can significantly deviate the UAV's path by simultaneously corrupting the GPS signals and forging control inputs without being detected by the UWB sensor. The prerequisite for the attack occurrence is first discussed. Based on this prerequisite, the optimal attack scheme is proposed, which maximizes the deviation between the nominal destination and the real one. Correspondingly, an energy-efficient and resilient navigation scheme based on Pontryagin's maximum principle [1] is formulated, which depresses the above covert attacker effectively. To sum up, this problem can be seen as a Stackelberg game [2] between a secure path planner (defender) and a covert attacker. The effectiveness and practicality of our theoretical results are illustrated via two series of simulation examples and a UAV experiment.

**Index Terms**—Covert attacks, Resilient path planning, Stackelberg game, UWB sensor

## I. INTRODUCTION

IN the last decade, the path planning of UAVs has gained considerations for its great potentials in search and rescue operations [3], wide-area supervision and measurement [4], and mobile smart sensors [5]. A well-known pioneering work [6], called minimum snap algorithm, was proposed to achieve energy-efficient but aggressive path planning for agile small UAVs. Although the above minimum snap scheme can generate smooth and energy-efficient polynomial trajectories, it is far from safe. The safety concept is quite diverse. However, two basic kinds of safety are concerned with robustness (against unintentional and stochastic uncertainties and disturbances) and resilience (against intentional smart attackers). Plenties of works (see [7] and references therein) have been proposed to resist harmful effects brought by uncertainties and disturbances. However, little work [8]–[10] has considered the resilience to the potential attacks, let alone covert ones [11, 12]. A novel zero-sum game-theoretic framework for analyzing and enhancing drone delivery systems' security was

This work was partially supported by the National Natural Science Foundation of China under Grant 61903258, 61973156, 61603180, Qatar National Research Fund NPRP12C-0814-190012, and the Tencent Rhinoceros Birds Scientific Research Foundation for Young Teachers of Shenzhen University.

<sup>\*</sup>These authors contribute equally and share the first authorship.

<sup>1</sup>Authors are with the Group Robotics with Intelligent Planning (GRIP) Lab, Department of Mechanical Engineering, University of Hong Kong, Hong Kong, {esmehe, gongxin}@connect.hku.hk

<sup>2</sup>Author is with the College of Mechatronics and Control Engineering, Shenzhen University, Shenzhen, 518060, China, cuiyukang@gmail.com

<sup>3</sup>Author is with Texas A&M University at Qatar, Doha, 23874, Qatar, tingwen.huang@qatar.tamu.edu

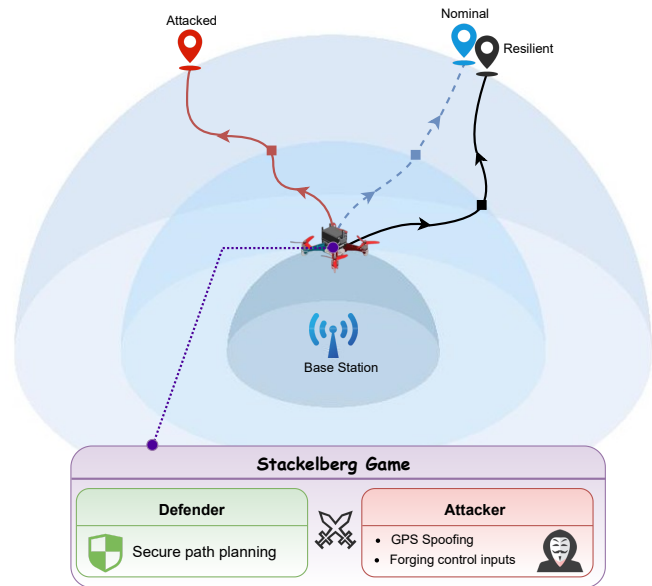


Fig. 1. The attack and defense scenario: The defender designs resilient control inputs to minimize the deviation between the nominal destination and attacked destination with the consideration of potential attackers. Then the attacker spoofs GPS signals and alters attack control inputs to maximize the above deviation according to the defense strategy. Essentially, the defender and attacker constitute the two players in a Stackelberg game, where the defender (leader) adopts her minimax strategy, that is, a resilient path planning scheme, whereas the attacker (follower) launches her countermeasure sequentially.

introduced in [8], where the vendor and attacker tried to minimize and maximize the delivery time, respectively. In [9], the resilient path planning against GPS spoofing attacks was achieved via the correction of other cooperative UAV neighbors, where the attack scheme was simple and detectable. Different from [8]–[10], a special kind of attacks, denoted as covert (undetectable) attacks [11, 12], may also exist under some special conditions, which could deviate the nominal path of UAVs without being detected by some correct-functioning sensors. Inspired by [11, 12], here we focus on the Ultra-Wideband (UWB) sensors, a special kind of 3D distance measurement units (3DMUs), which could only measure the distance between the Base Station (BS) and the UAV. An illustrative example is shown in Fig. 1: The attacked trajectory and the nominal one share the same time-varying distance w.r.t. the BS and thus cannot be detected abnormal by the onboard UWB sensor.

Various kinds of attacks in Cyber-Physical Systems have been reported in literature, including Denial of Service attacks [13], false injection attacks [14], replay attacks [15], man-in-the-middle (MITM) attacks [16, 17] and actuation attacks [18]. The MITM attacks on the GPS signal and the actuation attacks on the UAV motors are considered in this work. The danger induced by the MITM attacks on GPS systems (GPS spoofing

attacks) has gained substantial attention [16] for the wide applications of GPS positioning. It was reported in [17] that a UAV capture operation had been achieved via GPS spoofing attacks, where attack signals with higher power managed to displace the real GPS signals. However, the hoax of GPS spoofing attacks can be easily revealed by other onboard sensors. Here, we consider a special scenario in which the UAV is equipped with 3DMUs, such as UWB sensors. It is found that a covert attacker could still achieve her aim in such a scenario. Apart from the above GPS spoofing attacks, the actuation attacks on the UAV motors are also considered. The nominal control inputs are replaced by well-designed false control inputs, such that the UWB sensors can tell apart little difference between the readings during the nominal flight journey and the attacked one.

Unlike most of the above works, we focus on the path planning of the UAV platform under covert attacks, which cannot be detected by some well-functioning 3DMUs. This covert attack strategy is well-designed and thus cannot be easily tackled via the traditional attack detection and mitigation methods. Here, we formulate an integrated strategy pair consisting of optimal strategies for both the attacker and the defender. It is found that these two strategies essentially constitute the Nash equilibrium of a Stackelberg game. The main contributions of our work are summarized as follows:

- 1) The definition and characteristics of covert attacks on 3DMUs are given. The prerequisite for the covert attack occurrence in 3D space is further investigated.
- 2) An optimal attack strategy for the covert attacker is formulated such that the attacker can deviate the path of the UAV, while keeping it undetected by UWB sensors. Also, this kind of covert attack strategy can pose a threat on the UAV path planning in both single BS scenarios (SBS) and double BS scenarios (DBS), respectively.
- 3) An elaborate path planning strategy, based on Pontryagin's maximum principle, is proposed, anticipating the threat of covert attacks. Moreover, this strategy is feasible for both SBS and DBS.
- 4) The effectiveness of the above attack and defense scheme is illustrated via a series of numerical simulations. Also, an indoor UAV experiment is implemented, which shows the threat of the covert attacks and the practicality of our resilient path planning scheme.

**Notations:** The symbol  $\mathbb{R}$ ,  $\mathbb{N}$ ,  $\mathbb{R}_{>0}$  and  $\mathbb{R}_{\geq 0}$  denote the sets of real numbers, natural numbers, positive real numbers and nonnegative real numbers, respectively.  $0_{m \times n}$  denotes a zero matrix with  $m$  rows and  $n$  columns.  $I_n$  denotes an identity matrix with  $n$  dimensions. The superscript T means the transpose of a matrix.  $\mathbf{0}_m$  means a column vector of size  $m$  filled with 0.  $\|x\|$  denotes the 2-norm of vector  $x$ .  $\text{Rank}(M)$  represents the rank of the matrix  $M$ .  $\mathbf{e}_n^m \in \mathbb{R}^n$  denotes an unit vector with the length of  $n$ , whose  $m$ th element equals 1 and else elements equal 0. Denote the index set of sequential integers as  $\mathbf{I}(1, n) = \{1, 2, \dots, n\}$ . Let  $\vec{a}$ ,  $\vec{b}$  and  $\vec{c}$  denote three vectors with same dimensions,  $\vec{a} \perp \vec{b}$  and  $\vec{a} \parallel \vec{c}$  represent that  $\vec{a}$  is perpendicular to  $\vec{b}$  and  $\vec{a}$  is parallel to  $\vec{c}$ , respectively.  $\text{Proj}[\vec{a}, \vec{c}]$  means the projection of a vector  $\vec{a}$  on the direction

$\vec{c}$ .

## II. PRELIMINARY

### A. Problem Formulation

Consider the UAV model with triple-integrator dynamics:

$$\underbrace{\begin{bmatrix} \dot{p}_n \\ \dot{v}_n \\ \dot{a}_n \end{bmatrix}}_{\dot{x}_n} = \underbrace{\begin{bmatrix} 0_{3 \times 3} & I_3 & 0_{3 \times 3} \\ 0_{3 \times 3} & 0_{3 \times 3} & I_3 \\ 0_{3 \times 3} & 0_{3 \times 3} & 0_{3 \times 3} \end{bmatrix}}_A \underbrace{\begin{bmatrix} p_n \\ v_n \\ a_n \end{bmatrix}}_{x_n} + \underbrace{\begin{bmatrix} 0_{3 \times 3} \\ 0_{3 \times 3} \\ I_3 \end{bmatrix}}_B u_n, \quad (1)$$

where  $\bullet_n = [\bullet_{nx}, \bullet_{ny}, \bullet_{nz}]^T \in \mathbb{R}^3$ ,  $\bullet \in \{p, v, a, u\}$ , denotes the nominal position, velocity, acceleration and the control input (jerk) of the UAV in 3D space, respectively. We consider that the UAV is equipped with two kinds of sensors: a GPS sensor measuring the UAV's absolute position and a UWB sensor measuring the relative distance between the UAV and the  $n_b$  BS,  $n_b \in \mathbb{N}$ . Let  $b_i \in \mathbb{R}^3$  denote the position of the  $i$ th BS. The sensor readings are

$$y_n^{GPS} = p_n, \quad y_{n,i}^{UWB} = (p_n - b_i)^T (p_n - b_i). \quad (2)$$

We consider the UAV is flying in presence of an attacker who can spoof GPS signals and compromise nominal control inputs  $u_n$ . The dynamics of the attacked UAV is

$$\dot{x} = Ax + Bu, \quad (3)$$

where  $x \triangleq [p^T, v^T, a^T]^T$  and  $\bullet = [\bullet_x, \bullet_y, \bullet_z]^T \in \mathbb{R}^3$ ,  $\bullet \in \{p, v, a, u\}$ , denotes the exact UAV position, velocity, acceleration, and control inputs under attacks, respectively. The input saturation is considered such that  $\|u\| \leq \bar{u}$  with  $\bar{u} \in \mathbb{R}_{>0}$ , so is  $\|u_n\|$ . The sensor readings under attacks are

$$y_n^{GPS} = p + u^{GPS}, \quad y_n^{UWB} = (p - b_i)^T (p - b_i), \quad (4)$$

where  $u^{GPS} \in \mathbb{R}^3$  is the spoofing GPS signal.

Throughout this letter, the following assumption is valid.

*Assumption 1:* 1) All BS are located on the XY-plane ( $z = 0$ ); 2) there exists no coincident BS, that is,  $b_i \neq b_j, \forall i \neq j$ ; 3) the UAV flies in only one open half-space divided by the XY-plane; 4) there exists no three collinear BS; 5) at the initial time instant,  $x_n(0) = x(0)$ .

This letter depicts the conflict between the path planner (defender) and the attacker as a Stackelberg game. The defender (leader) tries to minimize the deviation between the attacked destination and the nominal one, anticipating that the attacker always adopts its best response. And the attacker (follower) alters its attack signals sequentially based on the defender strategy. To be more specific, the objectives of the attack scheme ( $u, u^{GPS}$ ) are:

- 1) maximizing the deviation between the nominal and the attacked path of the UAV;
- 2) evading detection by the well-functioning UWB sensors.

Correspondingly, the defender tries to devise resilient control inputs  $u_n$  such that

- 1) The UAV can minimize its integrated objective functions, including the energy consumption and destination deviation;

2) The UAV could detect the abnormality when a non-covert attack compromises the UAV.

Inspired by [11], we give the definition of covert attacks in 3D environment.

*Definition 1:* Under the above setting, the attack  $(u, u^{GPS})$  is called covert if and only if the measurements satisfy

$$y^{GPS} = y_n^{GPS}, \quad (5)$$

$$y^{UWB} = y_n^{UWB}, \quad (6)$$

during the whole flight journey.

### B. Prerequisite for Covert-attack Occurrence

Let  $s_{n,i} = p_n - b_i$  and  $s_i = p - b_i$  denote the UAV's nominal and attacked relative positions w.r.t. the  $i$ th BS, respectively. Denote  $R(p_n) = [s_{n,1}, s_{n,2}, \dots, s_{n,n_b}] \in \mathbb{R}_{3 \times n_b}$ , where  $n_b$  is the number of BS.

*Lemma 1:* Under Assumption 1, the covert attack  $(u, u^{GPS})$  exists if  $\text{Rank}(R(p_n(t))) \leq 2$ ,  $\exists t$ .

**Proof.** Lemma 1 is proven via Reduction to Absurdity. In other words, we try to show that all covert attacks subject to  $u = u_n$  under the condition that  $\text{Rank}(R(p_n(t))) \geq 3$ ,  $\forall t$ . From the assumption that  $x_n(0) = x(0)$ , we have  $s_i(0) = s_{n,i}(0)$ ,  $\forall i = \mathbf{I}(1, n_b)$ . By recalling Definition 1, covert attacks require that  $\dot{y}_i^{UWB} - \dot{y}_{n,i}^{UWB} = v^T s_i - v_n^T s_{n,i} = 0$ . Or equivalently,  $(v(\tau) - v_n(\tau))^T [s_{n,i}(\tau) \ s_{n,j}(\tau) \ s_{n,k}(\tau)] = 0$ ,  $\forall i, j, k \in \mathbf{I}(1, n_b)$ . Since  $\text{Rank}(R(p_n(t))) \geq 3$ , it follows that  $s_{n,i}(\tau)$ ,  $s_{n,j}(\tau)$  and  $s_{n,k}(\tau)$  are linearly independent to each other. Hence, we have  $v(\tau) = v_n(\tau)$  and thus  $s(\tau_+) = s_n(\tau_+)$ . By repeating the above process, we obtain that  $u = u_n$ ,  $\forall t$ , which means that no covert attack exists. This arouses a contradiction. Consequently, Lemma 1 is proven.  $\square$

Then we discuss attack and defense strategies in SBS ( $\text{Rank}(R) = 1$ ) and DBS ( $\text{Rank}(R) = 2$ ), respectively.

## III. ATTACK AND DEFENSE STRATEGIES IN SBS

### A. Characterization of Covert Attacks

For convenience, assume that the BS is located at the origin of the world coordinate, that is,  $b_1 = \mathbf{0}_3$ . Thus, (2) and (4) can be simplified as

$$y_n^{GPS} = p_n, \quad y_n^{UWB} = p_n^T p_n; \quad (7)$$

$$y^{GPS} = p + u^{GPS}, \quad y^{UWB} = p^T p. \quad (8)$$

*Lemma 2 (Implicit Characterization of Covert Attacks):* Covert attacks  $(u, u^{GPS})$  can only be achieved when

$$u^T p = u_n^T p_n + 3a_n^T v_n - 3a^T v, \quad u^{GPS} = p_n - p. \quad (9)$$

**Proof.** Taking third-order time derivative on both sides of (6), we arrive at

$$\ddot{y}^{UWB} - \ddot{y}_n^{UWB} = 2u^T p + 6a^T v - 2u_n^T p_n - 6a_n^T v_n = 0.$$

The proof is completed.  $\square$

Based on Lemma 2, we obtain:

*Corollary 1 (Explicit Characterization of Covert Attacks):* Every covert attack  $(u, u^{GPS})$  must satisfy

$$u = j_r p + w, \quad u^{GPS} = p_n - p, \quad (10)$$

with

$$j_r = \frac{u_n^T p_n + 3a_n^T v_n - 3a^T v}{\|p\|^2},$$

where  $j_r p = \text{Proj}[u, p]$ ,  $w = u - \text{Proj}[u, p]$ . It follows that  $w^T(t)p(t) = 0$ ,  $\forall t$ .

*Remark 1:* Corollary 1 provides a systematic approach to design covert attacks. The magnitude of  $w$  can be arbitrarily selected as long as  $\|u\| \leq \bar{u}$ , since it does not affect the covertness of attacks.

### B. Design of Optimal Covert Attacks

Based on Corollary 1, the optimal control problem is formulated as:

$$\max_w \|p(T) - p_n^F\|, \quad (11)$$

$$\text{s.t. } \dot{x} = Ax + Bu, \quad (11a)$$

$$u = j_r p + w, \quad (11b)$$

$$j_r = \frac{u_n^T p_n + 3a_n^T v_n - 3a^T v}{\|p\|^2}, \quad (11c)$$

$$\|u\| \leq \bar{u}. \quad (11d)$$

*Theorem 1 (Optimal Attack Strategy in SBS):* An optimal solution to the problem (11) is given as

$$w^* = j_t^* W_1 x,$$

with

$$\begin{cases} j_t^* = -\text{sgn}(\lambda^T B W_1 x) \sqrt{(\bar{u}^2 / \|p\|^2 - j_r^2)}, \\ W_1 = \begin{bmatrix} \frac{V_1}{\|V_1\|} & 0_{3 \times 3} & 0_{3 \times 3} \end{bmatrix}, \\ V_1 = \begin{bmatrix} 0 & p_{n_y}^F p_x - p_{n_x}^F p_y & p_{n_z}^F p_x - p_{n_x}^F p_z \\ p_{n_x}^F p_y - p_{n_y}^F p_x & 0 & p_{n_z}^F p_y - p_{n_y}^F p_z \\ p_{n_x}^F p_z - p_{n_z}^F p_x & p_{n_y}^F p_z - p_{n_z}^F p_y & 0 \end{bmatrix}, \end{cases}$$

where  $p_n^F$  denotes the destination of the nominal path. Furthermore,  $\lambda$  and  $x$  satisfy the following equations

$$\begin{cases} \dot{x} = Ax + B(j_r p + w^*), \\ -\dot{\lambda} = (A^T \lambda + j_r \tilde{P} \lambda + j_t^* \tilde{W}_1 \lambda) \\ \quad + (x^T \tilde{P} \lambda + 2j_r \kappa \|p\|^2) \nabla_x j_r, \end{cases}$$

where

$$P = [I_3 \quad 0_{3 \times 3} \quad 0_{3 \times 3}], \quad \tilde{P} = P^T B^T, \quad \tilde{W}_1 = W_1^T B^T, \\ \kappa = -\frac{\lambda^T B W_1 x}{2j_t^* \|p\|^2}, \quad \nabla_x j_r = 2\|p\|^{-2} [\mathbf{0}_3^T, \mathbf{0}_3^T, a^T]^T,$$

with  $\nabla_x j_r$  denoting the gradient of  $j_r$  w.r.t.  $x$ .

Moreover, the boundary conditions are

$$x(0) = x_n(0), \quad \lambda(T) = -2[(p(T) - p_n^F)^T, \mathbf{0}_3^T, \mathbf{0}_3^T]^T.$$

**Proof.** We rewrite the attacked control inputs (11b) in the form

$$u = j_r P x + \frac{1}{\sqrt{1+r^2}} j_t W_1 x + \frac{r}{\sqrt{1+r^2}} j_t W_2 x, \quad (12)$$

where

$$\begin{cases} W_2 = \begin{bmatrix} \frac{V_2}{\|V_2\|} & 0_{3 \times 3} & 0_{3 \times 3} \end{bmatrix} \in \mathbb{R}^{3 \times 9}, \\ V_2 = \begin{bmatrix} 0 & -p_{nz}^F l & p_{ny}^F l \\ p_{nz}^F l & 0 & -p_{nx}^F l \\ -p_{ny}^F l & p_{nx}^F l & 0 \end{bmatrix}, \\ l = p_x^2 + p_y^2 + p_z^2. \end{cases}$$

Let  $S_p$  be the plane consisting the BS location  $b_1$ , the UAV's current position  $p$ , and nominal destination  $p_n^F$ . In (12),  $Px = p$ ,  $W_1x$  satisfies  $W_1x \parallel S_p$  and  $W_1x \perp Px$ , and  $W_2x$  satisfies  $W_2x \perp S_p$  and  $W_2x \perp Px$ ;  $r$  is the ratio of the input magnitudes along  $W_2x$  and  $W_1x$  directions;  $j_t$  denotes the variable to be optimized. To derive the optimality conditions for (11), the Hamiltonian is defined as

$$\begin{aligned} H(x, j_t, r, \lambda, t) = & \lambda^T (Ax + B(j_r Px + \frac{1}{\sqrt{1+r^2}} j_t W_1x \\ & + \frac{r}{\sqrt{1+r^2}} j_t W_2x)), \end{aligned}$$

where  $\lambda(t) : [0, T] \rightarrow \mathbb{R}^9$  is a costate vector. Moreover, we rewrite the condition (11d) as

$$j_r^2 \|p\|^2 + j_t^2 \|p\|^2 \leq \bar{u}^2 \quad (13)$$

By adjoining the Hamiltonian with (13), we obtain the the Lagrangian:

$$\begin{aligned} L(x, j_t, r, \lambda, t, \kappa) = & H(x, j_t, r, \lambda, t) + \kappa(j_r^2 \|p\|^2 \\ & + j_t^2 \|p\|^2 - \bar{u}^2), \end{aligned}$$

where  $\kappa$  is a Lagrange multiplier related to the constraint (13).

From Pontryagin's maximum principle, the Hamiltonian is optimized via

$$\begin{aligned} j_t^* = & -\text{sgn}(\lambda^T B (\frac{1}{\sqrt{1+r^2}} W_1x + \frac{r}{\sqrt{1+r^2}} W_2x)) \\ & \times \sqrt{\frac{\bar{u}^2}{\|p\|^2} - j_r^2}. \end{aligned}$$

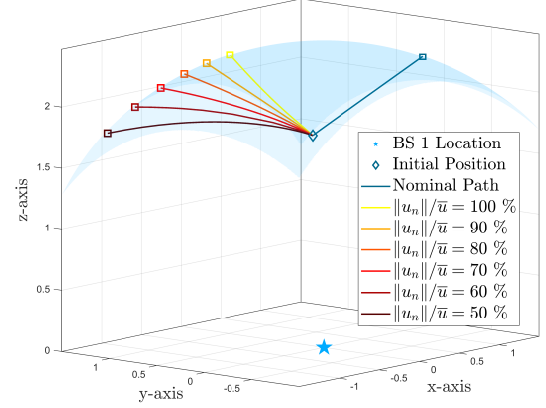
Moreover, the Pontryagin's maximum principle yields that

$$\begin{cases} \dot{x} = \frac{\partial L}{\partial \lambda} = Ax + B j_r Px + B j_t (\frac{1}{\sqrt{1+r^2}} W_1 + \frac{r}{\sqrt{1+r^2}} W_2)x, \\ -\dot{\lambda} = \frac{\partial L}{\partial x} = A^T \lambda + j_r P^T B^T \lambda + x^T P^T B^T \lambda \nabla_x j_r \\ \quad + j_t (\frac{1}{\sqrt{1+r^2}} W_1 + \frac{r}{\sqrt{1+r^2}} W_2)^T B^T \lambda + 2 j_r \kappa \|p\|^2 \nabla_x j_r, \\ \frac{\partial L}{\partial j_t} = \lambda^T B (\frac{1}{\sqrt{1+r^2}} W_1 + \frac{r}{\sqrt{1+r^2}} W_2)x + 2 \kappa j_t \|p\|^2 = 0, \\ \frac{\partial L}{\partial r} = j_t \lambda^T B (-\frac{r}{(\sqrt{1+r^2})^3} W_1x + \frac{1}{(\sqrt{1+r^2})^3} W_2x) = 0. \end{cases}$$

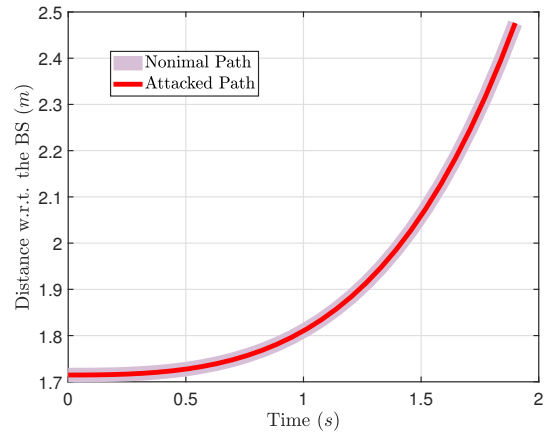
First, it is easy to find that  $r = 0$  is a feasible solution to  $\frac{\partial L}{\partial r} = 0$  since  $(-r W_1x + W_2x) = 0$ . Then we show that  $\frac{\partial L}{\partial r} = 0$  cannot hold when  $r \neq 0$ . Under this condition, the assertion  $\frac{\partial L}{\partial r} = 0$  leads to the assertion  $B^T \lambda \parallel Px$ , since  $Px$ ,  $W_1x$  and  $W_2x$  are perpendicular to each other. Since  $B^T \lambda \parallel Px$  cannot hold all the times, it follows that the assertion  $r = 0$  is needed for the optimal attacks. The transversality condition is  $\lambda(T) = -\frac{\partial}{\partial x} \|p(T) - p_n^F\|$ . By employing  $r = 0$ , we obtain the rest part of this theorem.  $\square$

A simulation example is given in Fig. 2.

*Remark 2:* The maximal deviation of a UAV between its nominal and attacked destination  $\|p_n^F - p^F\|$  is achieved when the attacker only focuses on the direction along  $W_1x$ .



(a) Attack performance



(b) UWB sensor readings along both nominal and attacked paths

Fig. 2. Covert attacks in SBS with simulation parameters  $T = 1.9s$ ,  $v(0) = 0m/s$ ,  $a(0) = 0m/s^2$  and  $u_n = [0.5, -0.5, 0.5]^T$ : (a) For a given nominal path (blue line), a series of attacked trajectories is obtained from Theorem 1 with different  $\bar{u}$ . As the  $\bar{u}$  increases, the deviation induced by optimal attack enlarges significantly. The light blue sphere represents that all destinations of the UAV under attacks share the same distance to the BS as the nominal destination. (b) Taking the condition that  $\|u_n\|/\bar{u} = 70\%$  for example, the UWB sensor readings of the attacked path always equals to the readings of the nominal path, satisfying Definition 1.

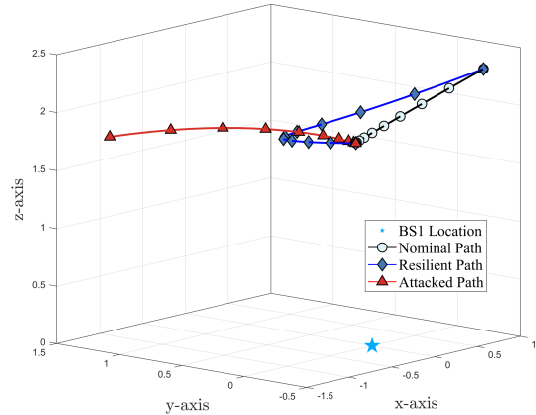


Fig. 3. Defense in SBS with simulation parameters  $\epsilon = 1$ ,  $\|u_n\|/\bar{u} = 50\%$ : For the nominal path (black line), it can be compromised as the attacked path (red line). By employing the resilient path planning scheme in Theorem 2, the UAV moves along the resilient path (blue line) and reaches the nominal destination with little tolerance.

### C. Resilient Path Planning Scheme

**Lemma 3 (Resilient Control Inputs in SBS):** Let  $\mathbb{S} : \mathbb{R}_{\geq 0} \rightarrow \{-1, 1\}$  denote a double-value function family. Under Assumption 1, the defense strategy is resilient if there exists a function  $\zeta \in \mathbb{S}$  such that

$$u_n = \zeta \frac{p_n}{\|p_n\|} \bar{u}. \quad (14)$$

**Proof.** Consider the time instant  $\tau = 0$ . It follows from Assumption 1 and (9) that

$$u_n^T(\tau) p_n(\tau) = u^T(\tau) p(\tau). \quad (15)$$

By substituting (14) into (15) and then taking the 2-norm on both sides, we obtain

$$\begin{aligned} \bar{u} \|p_n(\tau)\| &= |u_n(\tau)^T p_n(\tau)| = |u^T(\tau) p(\tau)| \\ &= \bar{u} \|p(\tau)\|. \end{aligned} \quad (16)$$

From Cauchy-Schwarz inequality, we have  $|\langle u(\tau), p(\tau) \rangle| \leq \|u(\tau)\| \cdot \|p(\tau)\|$ . To achieve (16),  $u(\tau)$  and  $p(\tau)$  should be linearly dependent and  $\|u(\tau)\| = \bar{u}$ .

Thus, we have

$$u(\tau) = \sigma(\tau) \frac{p(\tau)}{\|p(\tau)\|} u_{max}.$$

where  $\sigma(\tau) \in \mathbb{S}$ . To be noticed, if  $\sigma(\tau) \neq \zeta(\tau)$ , (15) is not satisfied. Thus,  $u(\tau) = u_n(\tau)$ . Consequently,  $p_n(\tau^+) = p(\tau^+)$ . By repeating the above process, we obtain that  $p = p_n, \forall t$ , which verifies the resilience of (14).  $\square$

A Stackelburg game framework from the viewpoint of the defender is considered in (17), whose objective function is a weighted combination of the destination deviation and the energy consumption throughout the flight:

$$\min_{u_n, T} \max_w \epsilon \int_0^T u_n^T u_n dt + \|p_n(T) - p_n^F\|, \quad (17)$$

$$\text{s.t. } \dot{x}_n = Ax_n + Bu_n, \quad (17a)$$

$$u_n = j_r p_n + w, \quad (17b)$$

where  $\epsilon$  is a weight to adjust the importance of the above two objectives. From Lemma 3, we obtain that the resilient control is achieved via keeping  $w = 0$ . Therefore, we simplify the game in (17) into an unilateral optimization problem:

$$\min_{u_n, T} \epsilon \int_0^T u_n^T u_n dt + \|p_n(T) - p_n^F\|, \quad (18)$$

$$\text{s.t. } \dot{x}_n = Ax_n + Bu_n, \quad (18a)$$

$$u_n = j_r p_n, \quad (18b)$$

$$j_r = \zeta \frac{\bar{u}}{\|p_n\|}, \quad (18c)$$

**Theorem 2 (Optimal defense Strategy in SBS):** Let  $u_n^*$  and  $T^*$  be the optimal solution to (18), we have

$$u_n^* = \zeta^* \frac{p_n}{\|p_n\|} \bar{u}, \quad T^* = \xi.$$

where

$$\zeta^* = -\text{sgn}(\lambda^T B p_n). \quad (19)$$

$x_n, \lambda$  and  $\xi$  satisfy

$$\begin{cases} \dot{x}_n = \xi(Ax_n + \frac{\zeta^* \bar{u}}{\|p_n\|} B p_n), \\ -\dot{\lambda} = \xi(A^T \lambda + \frac{\zeta^* \bar{u}}{\|p_n\|^3} \phi(p_n)^T B^T \lambda), \\ \dot{\xi} = 0, \end{cases} \quad (20)$$

where  $\phi(p_n) = \|p_n\|^2 P - p_n p_n^T P$ .

For  $t \in [0, 1]$ , boundary conditions are

$$\begin{cases} x_n(0) = x_I, \\ \lambda(1) = -2 [((p_n(1) - p_n^F)^T, \mathbf{0}^T, \mathbf{0}^T)^T], \\ \lambda(0)(Ax_0 + B\zeta^*(0) \frac{p_n(0)}{\|p_n(0)\|} \bar{u}) = -\epsilon \bar{u}^2. \end{cases}$$

**Proof.** To compute the unknown final time  $T$ , we define  $t = \xi\tau$ , with  $\xi \in \mathbb{R}_{>0}$  denoting a constant scalar to be determined and  $\tau \in [0, 1]$  denoting a new time scale [19, Equation 16, Page 276]. Thus, we select the following Hamiltonian:

$$H(x_n, j_r, \lambda) = \epsilon \bar{u}^2 + \xi \lambda^T (Ax_n + B j_r P x_n),$$

with  $\lambda$  denoting a costate vector.

By recalling Pontryagin's maximum principle, we have

$$\begin{cases} \dot{x}_n = \frac{\partial H}{\partial \lambda} = \xi(Ax_n + Bu_n), \\ -\dot{\lambda} = \frac{\partial H}{\partial x} = \xi(A^T \lambda + \frac{\partial u_n}{\partial x_n}^T B^T \lambda). \end{cases} \quad (21)$$

Based on constraint (18c), the Hamiltonian is optimized via

$$j_r^* = -\text{sgn}(\lambda^T B p_n) \frac{\bar{u}}{\|p_n\|}, \quad (22)$$

which leads to the expression of  $\zeta^*$  in (19).

By recalling that  $P x_n$  equals to  $p_n$ , we rewrite (14) as

$$u_n = \zeta \frac{P x_n}{\|P x_n\|} \bar{u}. \quad (23)$$

Hence, we compute that

$$\frac{\partial u_n}{\partial x_n} = \frac{\zeta \bar{u}}{\|p_n\|} P - \frac{\zeta \bar{u}}{\|p_n\|^3} P x_n x_n^T P^T P. \quad (24)$$

By substituting (23) and (24) into (21), we obtain (20).

The additional unknown parameter  $\xi$  can be determined from the fact that the Hamiltonian  $H(x_n, u_n, \lambda)$  stays constant along the path [19, Equation 10, Page 276]. The transversality condition for the final time is  $H|_{t_f} = 0$ . Hence, along the entire path there is  $H = 0$ . By applying this condition to the time instant  $t = 0$ , we obtain  $H|_{t_0} = 0$ . By recalling that  $H(x_n(0), \zeta(0), \lambda(0)) = 0$ , the initial boundary conditions can be obtained.

The proof is completed.  $\square$

A simulation example is given in Fig. 3.

## IV. ATTACK AND DEFENSE STRATEGIES IN DBS

### A. Covert Attacks in DBS

Now, we consider the optimal attacks launched in DBS. The locations of the two BS are  $b_1 = \mathbf{0}_3$  and  $b_2 = [b_x, 0, 0]^T$ .

**Lemma 4:** Every covert attack  $(u, u^{GPS})$  must satisfy

$$\begin{cases} p^T p = p_n^T p_n, & b_2^T p = b_2^T p_n, \\ v^T p = v_n^T p_n, & b_2^T v = b_2^T v_n, \\ a^T p + v^T v = a_n^T p_n + v_n^T v_n, & b_2^T a = b_2^T a_n. \end{cases}$$

**Proof.** To get above equations, we take the time derivative on both sides of the equality  $s_{n,i}^T s_{n,i} = s_i^T s_i$ . By recalling the assumption  $s_{n,i}(0) = s_i(0)$ , we get  $2\dot{p}^T p = 2\dot{p}_n^T p_n$ ,  $-2b_2^T \dot{p} = -2b_2^T \dot{p}_n$ . Similarly, taking derivative on both sides of the equality  $v^T p = v_n^T p_n$ ,  $-b_2^T v = -b_2^T v_n$ , we obtain  $\dot{v}^T p + v^T \dot{p} = \dot{v}_n^T p_n + v_n^T \dot{p}_n$ ,  $-b_2^T \dot{v} = -b_2^T \dot{v}_n$ .  $\square$

*Lemma 5 (Implicit Characterization of Covert Attacks):* In DBS, covert attacks  $(u, u^{GPS})$  can only be achieved when

$$\begin{aligned} Cu + \mathbf{e}_2^T u^T D_1 p + 3\mathbf{e}_2^T a^T D_1 v = Cu_n + \mathbf{e}_2^T u_n^T D_1 p_n \\ + 3\mathbf{e}_2^T a_n^T D_1 v_n, \\ u^{GPS} = p_n - p, \end{aligned} \quad (25)$$

where  $C = [\mathbf{e}_2^T \mathbf{0}_2 \mathbf{0}_2]$ ,  $D_1 = [\mathbf{0}_3 \mathbf{e}_3^T \mathbf{e}_3^T]$ .

**Proof.** Taking third-order time derivative on both sides of (6), we arrive at

$$\begin{aligned} \ddot{y}_i^{UWB} - \ddot{y}_{n,i}^{UWB} = 2u^T p + 6a^T v - 2b_i^T u - 2u_n^T p_n \\ - 6a_n^T v_n + 2b_i^T u_n = 0. \end{aligned} \quad (26)$$

The proof is completed.  $\square$

From Lemma 4 and 5, we obtain  $\bullet_x = \bullet_{nx}$ ,  $\forall \bullet \in \{p, v, a, u\}$ , due to the augment of the second BS. Thus, we have:

*Corollary 2 (Explicit Characterization of Covert Attacks):* Covert attacks  $(u, u^{GPS})$  must satisfy

$$u = j_{r1} D_1 p + j_{r2} D_2 p + w, \quad u^{GPS} = p_n - p, \quad (27)$$

where  $D_2 p = \text{Proj}[p, b_2]$  and  $D_1 p = p - D_2 p$ , respectively.  $j_{r1}$  and  $j_{r2}$  are variables concerned about the input magnitude along the  $D_1 p$  and  $D_2 p$  directions:

$$\begin{aligned} j_{r1} = \frac{u_n^T D_1 p_n + 3a_n^T D_1 v_n - 3a^T D_1 v}{p^T D_1 p}, \quad j_{r2} = \frac{D_3 u_n}{D_3 p} \\ D_2 = [(\mathbf{e}_3^1)^T, \mathbf{0}_3^T, \mathbf{0}_3^T], \quad D_3 = (\mathbf{e}_3^1)^T. \end{aligned}$$

$w$  is the projection of the control input on the direction perpendicular to both  $D_1 p$  and  $D_2 p$  directions, that is,  $w^T D_i p = 0$ ,  $i \in \mathbf{I}(1, 2)$ ,  $\forall t$ .

Based on Corollary 2, the optimal attack problem is formulated as:

$$\max_w \quad \|p(T) - p_n^F\|, \quad (28)$$

$$\text{s.t.} \quad \dot{x} = Ax + Bu, \quad (28a)$$

$$u = j_{r1} D_1 p + j_{r2} D_2 p + w, \quad (28b)$$

$$j_{r1} = \frac{u_n^T D_1 p_n + 3a_n^T D_1 v_n - 3a^T D_1 v}{p^T D_1 p}, \quad (28c)$$

$$j_{r2} = \frac{D_3 u_n}{D_3 p}, \quad (28d)$$

$$\|u\| \leq \bar{u}. \quad (28e)$$

*Theorem 3 (Optimal Attack Strategy for DBS):* An optimal solution to the problem (28) is given as

$$w^* = j_t^* W x,$$

where

$$j_t^* = -\text{sgn}(\lambda^T B W x) \sqrt{\frac{(\bar{u}^2 - j_{r1}^2 \|P_1 x\|^2 - j_{r2}^2 \|P_2 x\|^2)}{\|W x\|^2}}, \quad (29)$$

$$W = [V \mathbf{0}_{3 \times 3} \mathbf{0}_{3 \times 3}], \quad V = [\mathbf{0}_3 \quad -\mathbf{e}_3^3 \quad \mathbf{e}_3^2].$$

$\lambda$  and  $x$  satisfy

$$\begin{cases} \dot{x} = Ax + B(j_{r1} P_1 x + j_{r2} P_2 x + w^*), \\ -\dot{\lambda} = (A^T \lambda + j_{r1} \tilde{P}_1 \lambda + j_{r2} \tilde{P}_2 \lambda + j_t^* \tilde{W} \lambda) \\ \quad + (x^T \tilde{P}_1 \lambda + 2j_{r1} \kappa \|P_1 x\|^2) \nabla_x j_{r1} \\ \quad + (x^T \tilde{P}_2 \lambda + 2j_{r2} \kappa \|P_2 x\|^2) \nabla_x j_{r2}, \end{cases}$$

where

$$\begin{cases} P_i = [D_i \quad \mathbf{0}_{3 \times 3} \quad \mathbf{0}_{3 \times 3}], \quad \tilde{P}_i = P_i^T B^T, \\ \tilde{W} = W^T B^T, \quad \kappa = -\frac{\lambda^T B W x}{2j_t^* \|W x\|^2}, \\ \nabla_x j_{r1} = 2 \|P_1 x\|^{-2} [\mathbf{0}^T, \mathbf{0}^T, 0, a_y, a_z]^T, \\ \nabla_x j_{r2} = 2 \|P_2 x\|^{-2} [\mathbf{0}^T, \mathbf{0}^T, a_x, 0, 0]^T, \end{cases}$$

with  $\nabla_x j_{ri}$  denoting the gradient of  $j_{ri}$  w.r.t.  $x$ .

Boundary conditions are

$$x(0) = x_n(0), \quad \lambda(T) = -2[(p(T) - p_n^F)^T, \mathbf{0}_3^T, \mathbf{0}_3^T]^T.$$

**proof.** We write (28b) in the form that

$$u = j_{r1} P_1 x + j_{r2} P_2 x + j_t W x, \quad (30)$$

Similarly, we employ the following Hamiltonian

$$H(x, j_t, \lambda, t) = \lambda^T (Ax + B(j_{r1} P_1 x + j_{r2} P_2 x + j_t W x)),$$

with  $\lambda(t) : [0, T] \rightarrow \mathbb{R}^9$  denoting a costate vector.

We rewrite the constraint (28e) as

$$j_{r1}^2 \|P_1 x\|^2 + j_{r2}^2 \|P_2 x\|^2 + j_t^2 \|W x\|^2 \leq \bar{u}^2, \quad (31)$$

and the Lagrangian can be formulated by adjoining the Hamiltonian with (31):

$$\begin{aligned} L(x, j_t, \lambda, t, \kappa) = H(x, j_t, \lambda, t) \\ + \kappa (j_{r1}^2 \|P_1 x\|^2 + j_{r2}^2 \|P_2 x\|^2 + j_t^2 \|W x\|^2 - \bar{u}^2), \end{aligned}$$

where  $\kappa$  is a Lagrange multiplier related to (31).

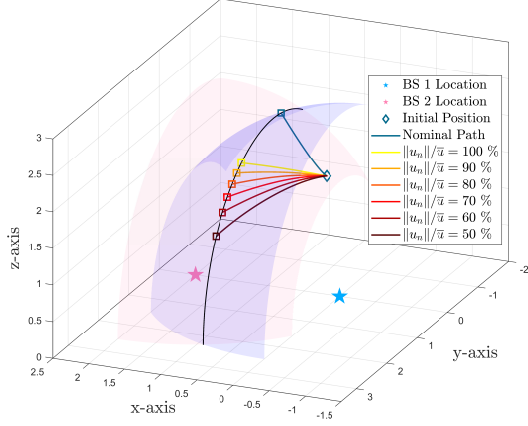
From Pontryagin's maximum principle, the Hamiltonian is optimized via  $j_t^*$  subject to the constraint (31). Hence, we obtain the optimal control law (29). The Pontryagin's maximum principle yields that

$$\begin{cases} \dot{x} = \frac{\partial L}{\partial \lambda} = Ax + B j_{r1} P_1 x + B j_{r2} P_2 x + B j_t W x, \\ -\dot{\lambda} = \frac{\partial L}{\partial x} = A^T \lambda + j_{r1} P_1^T B^T \lambda + x^T P_1^T B^T \lambda \nabla_x j_{r1} \\ \quad + j_{r2} P_2^T B^T \lambda + x^T P_2^T B^T \lambda \nabla_x j_{r2} + j_t W^T B^T \lambda \\ \quad + 2j_{r1} \kappa \|P_1 x\|^2 \nabla_x j_{r1} + 2j_{r2} \kappa \|P_2 x\|^2 \nabla_x j_{r2}, \\ \frac{\partial L}{\partial j_t} = \lambda^T B W x + 2\kappa j_t \|W x\|^2 = 0. \end{cases}$$

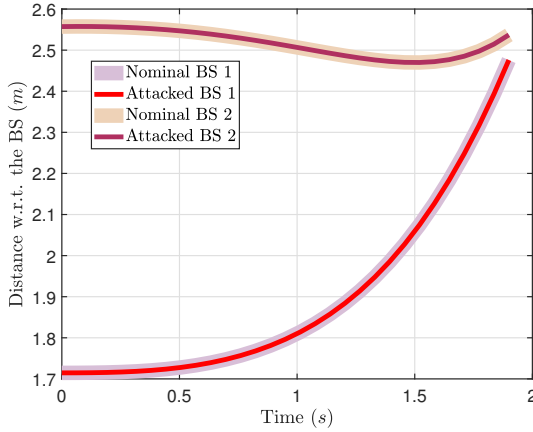
The transversality condition can be obtained via  $\lambda(T) = -\frac{\partial}{\partial x} \|p(T) - p_n^F\|$ .

The proof is completed.  $\square$

A simulation example is given in Fig. 4. Moreover, Fig. 5 shows the difference of the attack performance between SBS and DBS.



(a) Attack performance



(b) UWB sensor readings on both nominal and attacked paths

Fig. 4. Covert attacks in DBS with simulation parameters  $T = 1.9s$ ,  $v(0) = 0m/s$ ,  $a(0) = 0m/s^2$  and  $u_n = [0.5, -0.5, 0.5]^T$ : (a) The purple and pink surfaces represent two spherical surfaces centered by the BS 1 and 2, respectively. The radius of each surface equals to the distance between the nominal destination and the associated BS. Similar to the SBS, the bigger the upper bound of the inputs, the larger the deviation. It should be noticed that the BS 2 adds another constraint on the covert attacker. Consequently, the attacker could only drive the UAV in the intersecting line of two time-varying spheres centered by the BS all the time. The radius of each time-varying sphere equals to the distance between the nominal position at the same time instant and the associated BS. (b) Taking the condition that  $\|u_n\|/\bar{u} = 70\%$  for example, each sensor reading under attacks is always consistent with that in nominal environments, which shows the covertness of the attacker.

### B. Resilient Path Planning in DBS

**Lemma 6 (Resilient Control Inputs in DBS):** Under Assumption 1, the defense strategy is resilient if there exists a function  $\zeta \in \mathbb{S}$  satisfying

$$u_n = (\zeta D_1 p_n + D_2 p_n) \frac{\bar{u}}{\|p_n\|}. \quad (32)$$

**Proof.** Similar to SBS, from (26) and (32), we obtain

$$\begin{aligned} \frac{\bar{u} \|D_1 p_n(\tau)\|^2}{\|p_n(\tau)\|} &= |u_n(\tau)^T D_1^T D_1 p_n(\tau)| = |u^T(\tau) D_1^T D_1 p(\tau)| \\ &= \frac{\bar{u} \|D_1 p(\tau)\|^2}{\|p(\tau)\|}. \end{aligned} \quad (33)$$

By recalling the Cauchy-Schwarz inequality, we have  $|\langle D_1 u(\tau), D_1 p(\tau) \rangle| \leq \|D_1 u(\tau)\| \cdot \|D_1 p(\tau)\|$ . To achieve (33),

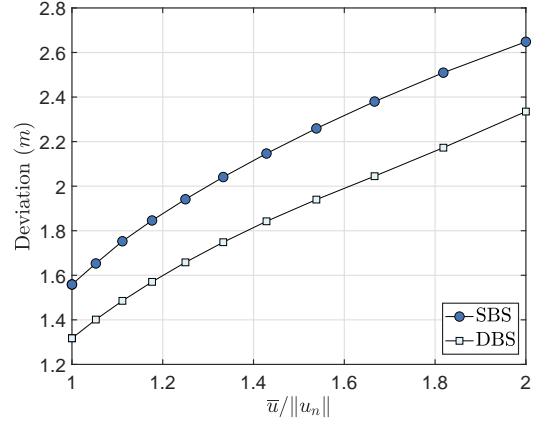


Fig. 5. The attacked deviation versus  $\bar{u}/\|u_n\|$ : The deviation w.r.t. the nominal destination enlarges as the  $\bar{u}/\|u_n\|$  increases. Notice that the deviation of the UAV in DBS is always smaller than that in SBS under the same  $\bar{u}/\|u_n\|$  condition, due to the additional constraint.

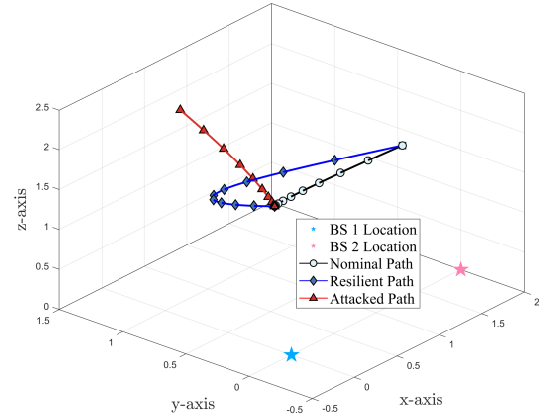


Fig. 6. Defense in DBS with simulation parameters  $\epsilon = 1$ ,  $\|u_n\|/\bar{u} = 70\%$ : Similar to the SBS, the UAV can reach the nominal destination with little tolerance by following the resilient strategy in Theorem 4. Without the resilient policy, the nominal path could be compromised as the attacked one (red line). Since there exists another BS adding constraint on the covert attacker, it is easier for the defender to achieve its target.

$D_1 u(\tau)$  and  $D_1 p(\tau)$  are considered to be linearly dependent and  $\|D_1 u(\tau)\| = \frac{\|D_1 p_n\|}{\|p_n\|} \bar{u}$ . Thus, we have

$$u(\tau) = (\zeta(\tau) D_1 p(\tau) + D_2 p(\tau)) \frac{\bar{u}}{\|p(\tau)\|}.$$

Thus,  $u(\tau) = u_n(\tau)$ . Consequently,  $p_n(\tau_+) = p(\tau_+)$ . By repeating the above process, we obtain that  $p = p_n, \forall t$ , which proves the resilience of (32).

The proof is completed.  $\square$

Following the similar analysis to the SBS, the Stackelberg game in (17) can be simplified into the following optimization scheme based on the resilient control law in Lemma 6:

$$\min_{u_n, T} \epsilon \int_0^T u_n^T u_n dt + \|p_n(T) - p_n^F\|, \quad (34)$$

$$\text{s.t. } \dot{x}_n = Ax_n + Bu_n, \quad (34a)$$

$$u_n = (\zeta D_1 p_n + D_2 p_n) \frac{\bar{u}}{\|p_n\|}. \quad (34b)$$

*Theorem 4 (Optimal Defense Strategy in DBS):* Let  $u_n^*$  and  $T^*$  be an optimal solution to (34),

$$u_n^* = (\zeta^* D_1 p_n + D_2 p_n) \frac{\bar{u}}{\|p_n\|}, \quad T^* = \xi.$$

where

$$\zeta^* = -\text{sgn}(\lambda^T B D_1 p_n). \quad (35)$$

$x_n$  and  $\lambda$  and  $\xi$  satisfy

$$\begin{cases} \dot{x}_n = \xi(Ax_n + \zeta^* \frac{\bar{u}}{\|p_n\|} B D_1 p_n + \frac{\bar{u}}{\|p_n\|} B D_2 p_n), \\ -\dot{\lambda} = \xi(A^T \lambda + \zeta^* \frac{\bar{u}}{\|p_n\|^3} \phi_1(p_n)^T B^T \lambda \\ \quad + \frac{\bar{u}}{\|p_n\|^3} \phi_2(p_n)^T B^T \lambda), \\ \dot{\xi} = 0 \end{cases} \quad (36)$$

where

$$\phi_i(p_n) = \|p_n\|^2 P_i - D_i p_n p_n^T P. \quad (37)$$

For  $t \in [0, 1]$ , boundary conditions are listed as

$$\begin{cases} x_n(0) = x_I, \quad \lambda(1) = -2[(p_n(1) - p_n^F)^T, \mathbf{0}_3^T, \mathbf{0}_3^T], \\ \lambda(0)(Ax_0 + B \frac{\bar{u}}{\|p_n(0)\|} (\zeta^*(0) D_1 p_n(0) + D_2 p_n(0))) = -\epsilon \bar{u}^2. \end{cases}$$

**Proof.** We define the Hamiltonian:

$$H(x_n, u_n, \lambda) = \epsilon \bar{u}^2 + \lambda^T \xi(Ax_n + Bu_n),$$

with  $\lambda$  denoting a costate vector.

By substituting (34b) into the above equation and following the Pontryagin's maximum principle, we obtain (35). Moreover, it is necessary that

$$\begin{cases} \dot{x}_n = \xi(Ax_n + Bu_n), \\ -\dot{\lambda} = \xi(A^T \lambda + \frac{\partial u_n}{\partial x_n}^T B^T \lambda), \\ \dot{\xi} = 0. \end{cases} \quad (38)$$

where

$$\begin{aligned} \frac{\partial u_n}{\partial x_n} &= \zeta \frac{\bar{u}}{\|P x_n\|} P_1 - \zeta \frac{\bar{u}}{\|P x_n\|^3} P_1 x_n x_n^T P^T P \\ &\quad + \frac{\bar{u}}{\|P x_n\|} P_2 - \frac{\bar{u}}{\|P x_n\|^3} P_2 x_n x_n^T P^T P. \end{aligned} \quad (39)$$

The expression of  $\phi_i(p_n)$  in (37) follows by substitution. (36) can be obtained by substituting (32) and (39) into (38).

The proof is completed.  $\square$

A simulation example is given in Fig. 6.

*Remark 3:* Different from the previous works [11, 12], we consider more complex and practical robot dynamics and 3DMUs (including UWB sensors). It should be noticed that the extension on the dimensionality is nontrivial for the reason of strong coupling among the three dimensions. Also, we focus on the optimization of the energy-consumption rather than time-consumption.

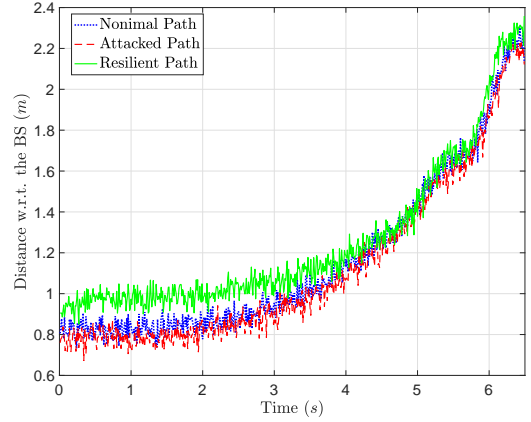


Fig. 7. UWB module reading in the experiment in  $0 \sim 6.5$  s: The attacked trajectory and the nominal one share the similar time-varying distances.

## V. EXPERIMENT VERIFICATION

We use a Q250 UAV, equipped with a Nooploop LinkTrack SS UWB Module [20], to conduct a resilient path planning experiment in SBS. A two-level controller scheme is employed, where the DJI Manifold 2-C and the Pixhawk 4 mini act as the upper and lower controllers, respectively. The Optitrack motion capture system acts as the GPS sensor since it could provide high-frequency and high-precision absolute position information. This information flow (a Robot Operating System (ROS) message) is replaced by another information flow (another ROS message) forged by the spoofing attacker. This attacker also alters the control inputs of the UAV to evade the detection by the well-functioning UWB module.

The experiment parameters are given as:  $\epsilon = 1$ ,  $\bar{u} = 0.084 \text{ m/s}^3$ ,  $u_n = [0.028, -0.028, 0.028]^T \text{ m/s}^3$ , and thus  $\|u_n\|/\bar{u} = 57.7\%$ . A Turtlebot 3 Robot acts as the BS, which is located at the Origin in the Optitrack coordinate. Moreover, the initial condition of the UAV is set as  $p(0) = [0.4, -0.3, -0.8]^T \text{ m}$ . The planning horizon is  $T = 6.5 \text{ s}$ .

Based on the above settings and parameters, we manage to conduct the experiment, whose video can be found at <http://147.8.138.175/wordpress/wp-content/uploads/gx/UWBdefense.mp4> and <https://youtu.be/IHbE0sJlqo>. As the video shows, the covert attacker can mislead the UAV from the nominal path to the attacked one, which implies her non-negligible threat on the path planning results. This threat could be relieved significantly by the resilient path planner. The attacker's covertness can be illustrated by the time-varying UWB sensor readings in Fig. 7. Three long exposure trajectories in the dark environment are recorded in Fig. 8, where the UAV is equipped with beacon lights in three colors.

## VI. CONCLUSION AND FUTURE WORK

This letter has addressed the problem of resilient path planning of a UAV under covert attacks. The definition and prerequisite for the covert attacks on the UWB sensors have been given. We show that such a covert attacker could deviate the UAV's path without being detected by the well-functioning



Fig. 8. Long exposure trajectories in the dark environment: The white, red and green flashes are the nominal, attacked and resilient trajectories, respectively.

UWB sensors. Then we have figured out the optimal attack scheme for both SBS and DBS, which shows that the threats brought by the attacker cannot be overlooked. Hence, we have proposed a resilient path planning algorithm by anticipating the potential covert attacker, which is verified via series of simulations and a UAV experiment. Essentially, the strategy pair of the resilient path planner and the attacker can be regarded as a Nash Equilibrium of a Stackelberg game. Future works will consider the sensor noise, and attack and defense mechanism in the UAV swarms [21].

## REFERENCES

- [1] I. M. Gelfand, R. A. Silverman, *et al.*, *Calculus of variations*. Courier Corporation, 2000.
- [2] T. Başar and G. J. Olsder, *Dynamic noncooperative game theory*. SIAM, 1998.
- [3] D. Kim, L. Xue, D. Li, Y. Zhu, W. Wang, and A. O. Tokuta, “On theoretical trajectory planning of multiple drones to minimize latency in search-and-reconnaissance operations,” *IEEE Trans. Mobile Comput.*, vol. 16, no. 11, pp. 3156–3166, 2017.
- [4] H. Kim, L. Mokdad, and J. Ben-Othman, “Designing UAV surveillance frameworks for smart city and extensive ocean with differential perspectives,” *IEEE Commun. Mag.*, vol. 56, no. 4, pp. 98–104, 2018.
- [5] T. M. Cabreira, C. Di Franco, P. R. Ferreira, and G. C. Buttazzo, “Energy-aware spiral coverage path planning for UAV photogrammetric applications,” *IEEE Robot. Autom. Lett.*, vol. 3, no. 4, pp. 3662–3668, 2018.
- [6] D. Mellinger and V. Kumar, “Minimum snap trajectory generation and control for quadrotors,” in *Proceedings of 2011 IEEE International Conference on Robotics and Automation*, 2011, pp. 2520–2525.
- [7] N. Dadkhah and B. Mettler, “Survey of motion planning literature in the presence of uncertainty: Considerations for UAV guidance,” *Journal of Intelligent & Robotic Systems*, vol. 65, no. 1, pp. 233–246, 2012.
- [8] A. Sanjab, W. Saad, and T. Başar, “Prospect theory for enhanced cyber-physical security of drone delivery systems: A network interdiction game,” in *Proceedings of 2017 IEEE International Conference on Communications*, 2017, pp. 1–6.
- [9] A. Eldosouky, A. Ferdowsi, and W. Saad, “Drones in distress: A game-theoretic countermeasure for protecting UAVs against GPS spoofing,” *IEEE Internet Things J.*, vol. 7, no. 4, pp. 2840–2854, 2019.
- [10] S. Banik and S. D. Bopardikar, “Secure route planning using dynamic games with stopping states,” *arXiv preprint arXiv:2006.07452*, 2020.
- [11] G. Bianchin, Y.-C. Liu, and F. Pasqualetti, “Secure navigation of robots in adversarial environments,” *IEEE Control Systems Letters*, vol. 4, no. 1, pp. 1–6, 2019.
- [12] Y.-C. Liu, G. Bianchin, and F. Pasqualetti, “Secure trajectory planning against undetectable spoofing attacks,” *Automatica*, vol. 112, p. 108655, 2020.
- [13] B. Duan, D. Yin, Y. Cong, H. Zhou, X. Xiang, and L. Shen, “Anti-jamming path planning for unmanned aerial vehicles with imperfect jammer information,” in *Proceedings of 2018 IEEE International Conference on Robotics and Biomimetics*. IEEE, 2018, pp. 729–735.
- [14] Y. Mo, E. Garone, A. Casavola, and B. Sinopoli, “False data injection attacks against state estimation in wireless sensor networks,” in *Proceedings of 49th IEEE Conference on Decision and Control*, 2010, pp. 5967–5972.
- [15] R. Langner, “Stuxnet: Dissecting a cyberwarfare weapon,” *IEEE Security Privacy*, vol. 9, no. 3, pp. 49–51, 2011.
- [16] D. P. Shepard, J. A. Bhatti, T. E. Humphreys, and A. A. Fansler, “Evaluation of smart grid and civilian UAV vulnerability to GPS spoofing attacks,” in *Proceedings of the 25th International Technical Meeting of The Satellite Division of the Institute of Navigation*, 2012, pp. 3591–3605.
- [17] A. J. Kerns, D. P. Shepard, J. A. Bhatti, and T. E. Humphreys, “Unmanned aircraft capture and control via GPS spoofing,” *J. Field Rob.*, vol. 31, no. 4, pp. 617–636, 2014.
- [18] S. Zuo and D. Yue, “Resilient output formation containment of heterogeneous multigroup systems against unbounded attacks,” *IEEE Trans. Cybern.*, 2020, doi: 10.1109/TCYB.2020.2998333.
- [19] G. Aly and W. Chan, “Numerical computation of optimal control problems with unknown final time,” *Journal of Mathematical Analysis and Applications*, vol. 45, no. 2, pp. 274–284, 1974.
- [20] H. Xu, L. Wang, Y. Zhang, K. Qiu, and S. Shen, “Decentralized visual-inertial-UWB fusion for relative state estimation of aerial swarm,” in *Proceedings of 2020 IEEE International Conference on Robotics and Automation*. IEEE, 2020, pp. 8776–8782.
- [21] A. Mustafa and H. Modares, “Attack analysis and resilient control design for discrete-time distributed multi-agent systems,” *IEEE Robot. Autom. Lett.*, vol. 5, no. 2, pp. 369–376, 2019.